

Hydrothermal synthesis and characterization of Eu^{3+} and Nd^{3+} -doped Bi_2O_3 nanomaterials

Marzieh sabaghian, Mahdi Behzad*, Shahin Khademinia

¹Department of Chemistry, Semnan University, Semnan, Iran

Article history:

Received: 15/Apr/2016

Received in revised form: 10/May/2016

Accepted: 20/May/2016

Abstract

Bi_2O_3 nanomaterials doped with Eu^{3+} and Nd^{3+} ions have been synthesized by a simple hydrothermal process at 180 °C for 48 h. $\text{Bi}(\text{NO}_3)_3 \cdot 5\text{H}_2\text{O}$ and KOH were used as raw materials. The as-prepared materials were characterized by X-ray diffraction (XRD). The data showed that the doped Bi_2O_3 materials were crystallized in a monoclinic crystal structure with space group of $\text{P}2_1/\text{c}$ and cell parameters of $a=5.8499 \text{ \AA}$, $b=8.1698 \text{ \AA}$ and $c=7.5123 \text{ \AA}$. The morphology of the obtained nanomaterials was investigated by field emission scanning electron microscope (FESEM). The morphology was remained unchanged after doping the rare elements into Bi_2O_3 . However, different morphology of the compounds was achieved. The FESEM images showed that the materials were composed of micro-nano rods, nanoparticles and flower structures. Elemental analyses of the doped nanomaterials were performed by energy-dispersive X-ray spectrometry (EDS). Also cell parameter refinements and interplanar spacing (d) of the obtained materials were investigated.

Keywords: Nanomaterials; Bismuth oxide; Neodymium; Europium; Hydrothermal method

1. Introduction

Bi_2O_3 is an important semiconductor. It has gained noticeable attention due to its good absorption capacity [1], dielectric permittivity, considerable photoconductivity, photoluminescence and high refractive index [2]. Because of these particular properties, Bi_2O_3 can be used in piezo-optic materials [3], superconductor ceramic glass manufacturing [4], solar cells [5], sensor optical coatings [6], oxide-ion conductors [7], bacteria inactivation and template-synthesis [8], photovoltaic cells [9], gas sensing [10], fuel cells [11] and photocatalysis [12]. Synthesis of bismuth oxides doped with Ce [13], Pr [14], Sm [15], Dy [16], Tb [17], Er [18, 19], Yb [20], Tm [21], Lu [22] and Ho [23] ions have been reported Previously.

Also, V^{5+} , Pb^{2+} , Ag^+ , Co^{2+} [24] and Fe^{3+} [25] doped bismuth oxides have been synthesized. In recent years, rare earth (RE) oxides have been used in ceramic industry and catalysis [26]. These materials show maximum power output, high chemical and thermal stability [27]. Among RE oxides, Nd_2O_3 has been widely used in luminescent and thermo luminescent materials [28, 29], photonic applications e.g. as phosphors providing yellow-to-violet up conversion emission [30], thin films [31] and protective coatings [32]. Also Eu^{3+} doped materials show the potential application for solar cells, photo luminescent properties [33-37], electrical conductivity [38, 39], photo catalytic activity [40, 41].

*.Corresponding author: E-mail address: mbehzad@semnan.ac.ir; Tel: +98-233 338 3195

However, to the best of our knowledge, there was no work has been devoted to Eu^{3+} and Nd^{3+} doped α - Bi_2O_3 via hydrothermal method. In this research, we have reported the hydrothermal synthesis of $\text{Bi}_{2-x}\text{Eu}_x\text{O}_3$ and $\text{Bi}_{2-x}\text{Nd}_x\text{O}_3$ nanomaterials. We have studied the elemental analysis and the effect of dopant amounts on the morphology of the synthesized nanomaterials.

2. Materials and methods

2.1. Synthesis of Eu^{3+} doped bismuth oxide ($x= 0.01, 0.03, 0.05, 0.07$ and 0.1 mmol)

Synthesis of Bismuth oxide as a typical experiment was performed according to the recently reported work [42]. Certain amounts of $\text{Bi}(\text{NO}_3)_3 \cdot 5\text{H}_2\text{O}$ (1.99, 1.97, 1.95, 1.93 or 1.9 mmol), Eu_2O_3 (0.01, 0.03, 0.05, 0.07 or 0.1 mmol, respectively), were dissolved in 50 mL of hot 1M KOH solution under magnetic stirring at 80 °C. The resultant solution was transferred into a 100-mL Teflon-lined stainless steel autoclave. The autoclave was sealed and maintained at 180°C for 48 h. When the reaction was completed, it was cooled to room temperature by water immediately, and then the resulting precipitate was recovered.

2.2. Synthesis of Nd^{3+} doped bismuth oxide ($x = 0.01, 0.03, 0.05, 0.07$ and 0.1 mmol)

Proper molar amounts of $\text{Bi}(\text{NO}_3)_3 \cdot 5\text{H}_2\text{O}$ (1.99, 1.97, 1.95, 1.93 or 1.9 mmol), Nd_2O_3 (0.01, 0.03, 0.05, 0.07 or 0.1 mmol, respectively), were dissolved in 50 mL of hot 1M KOH solution under magnetic stirring at 80 °C. The resultant solution was transferred into a 100-mL Teflon-lined stainless steel autoclave. The autoclave was sealed and maintained at 180 °C for 48 h. When the reaction was completed, it was cooled to room temperature by water immediately, and then the resulting precipitate was recovered.

2.3. Characterization

All chemicals including $\text{Bi}(\text{NO}_3)_3 \cdot 5\text{H}_2\text{O}$, KOH, Eu_2O_3 and Nd_2O_3 were of analytical grade and were obtained from Merck Company, Germany and used without further purifications. Phase identifications were performed on a powder X-ray diffractometer D5000 (Siemens AG, Munich, Germany) using $\text{CuK}\alpha$ radiation. The morphology of the obtained materials was examined with a field emission scanning electron microscope (Hitachi FE-SEM model S-4160) equipped with energy-dispersive X-ray (EDX) spectrometer. Cell parameter refinements were performed by Celref software version 3.

3. Results and discussion

3.1. Powder X-ray diffraction analysis

The crystal phases of the as synthesized materials were examined by powder X-ray diffraction technique. Figures 1 and 2 show the PXRD patterns of the Eu^{3+} , Nd^{3+} -doped bismuth oxide. It was found that the obtained materials were crystallized in monoclinic crystal structure with space group of $\text{P}2_1/\text{c}$ (ICCD PDF:41-1449). Besides, the intensive sharp diffractions propose that the as-synthesized materials are well crystallized. The theoretical doping limitations are 0-0.07 mmol of Eu^{3+} and 0-0.07 mmol of Nd^{3+} for bismuth oxide. However, for surplus mole% concentration of the dopant element, the impurity peaks were observed in the PXRD patterns. As shown in figure 1, the diffraction line at $2\theta \approx 29.3^\circ$ is assigned to the excess Eu_2O_3 [43]. The diffraction lines at $2\theta \approx 40.7^\circ$ and 57.5° in figure 2 are assigned to the excess Nd_2O_3 [27, 44].

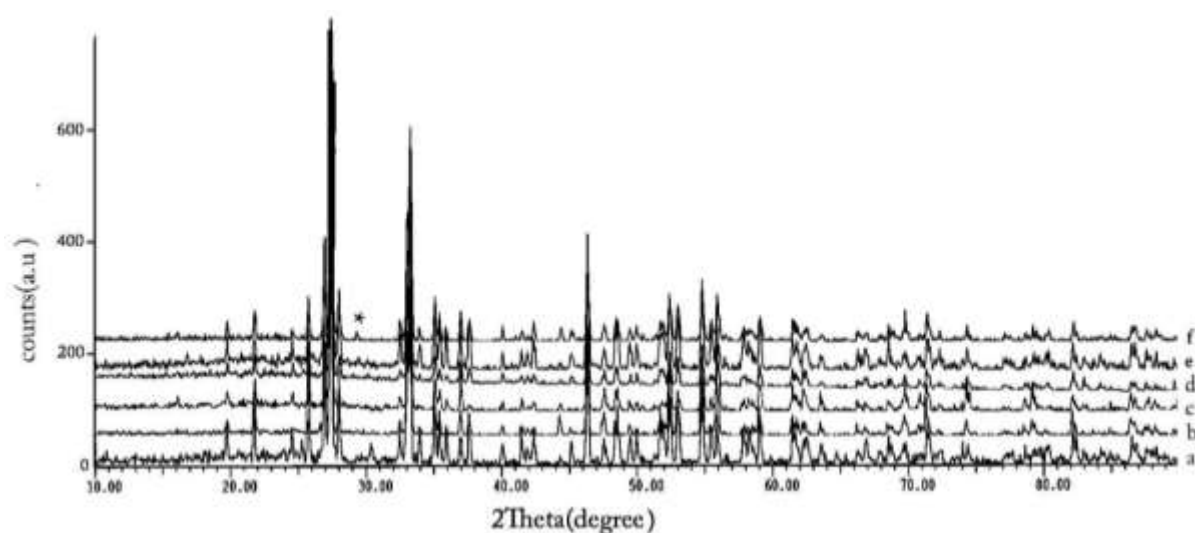


Fig. 1. XRD patterns of the synthesized $\text{Bi}_{2-x}\text{Eu}_x\text{O}_3$ nanoparticles, where (a) is $x=0\%$; (b) is $x=0.01$; (c) is $x=0.03$; (d) is $x=0.05$; (e) is $x=0.07$; (f) is $x=0.1$ mole%. * is due to Eu_2O_3 .

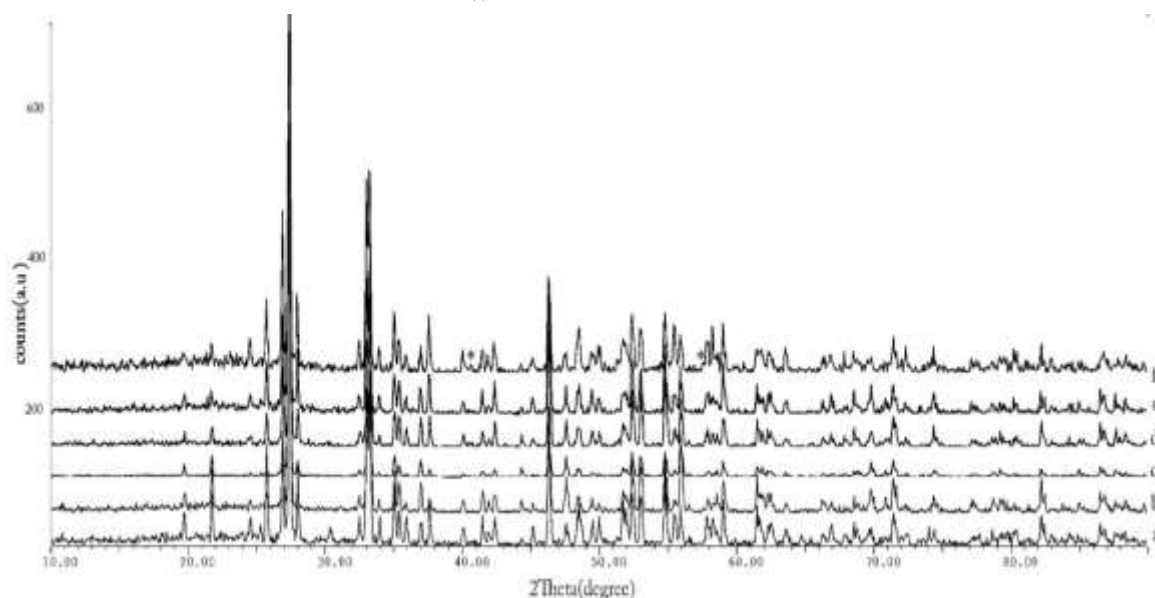


Fig. 2. XRD patterns of the synthesized $\text{Bi}_{2-x}\text{Nd}_x\text{O}_3$ nanoparticles, where (a) is $x=0\%$; (b) is $x=0.01$; (c) is $x=0.03$; (d) is $x=0.05$; (e) is $x=0.07$; (f) is $x=0.1$ mole%. * is due to Nd_2O_3 .

Cell parameter refinement data of the as synthesized nanomaterials are summarized in table 1. From table 1, it was found that parameters a, b and c for different mole percent of Eu^{3+} and Nd^{3+} doped Bi_2O_3 nanomaterials are smaller than those of the standard

sample. The average instrument errors were also investigated. It showed the difference among the parameters a-c refined by the celref software for sample (ICCD PDF: 41-1449) compared to doped materials.

Table 1. Cell parameters of Eu^{3+} and Nd^{3+} doped Bi_2O_3 nanomaterials. SD is the standard deviations.

Sample	a (SD)	b (SD)	c (SD)	V (\AA^3) (SD)
(JCPDS 41-1449)	5.8499	8.1698	7.5123	330.52
Pure Bi_2O_3	5.8323	8.1610	7.5058	328.77
0.01 mmol Eu^{3+}	(0.0052)	(0.0034)	(0.0068)	(0.461)
0.03 mmol Eu^{3+}	5.8405	8.1620	7.4999	329.31
0.05 mmol Eu^{3+}	(0.0083)	(0.0038)	(0.0099)	(0.706)
0.07 mmol Eu^{3+}	5.8406	8.1656	7.4990	329.03
0.01 mmol Nd^{3+}	(0.0145)	(0.0043)	(0.0183)	(1.249)
0.03 mmol Nd^{3+}	5.8632	8.1651	7.4983	331.28
0.05 mmol Nd^{3+}	(0.0165)	(0.0040)	(0.0181)	(1.342)
0.07 mmol Nd^{3+}	5.8482	8.1651	7.4996	329.89
0.01 mmol Nd^{3+}	(0.0048)	(0.0030)	(0.0045)	(0.371)
0.03 mmol Nd^{3+}	5.8447	8.1633	7.4945	329.31
0.05 mmol Nd^{3+}	(0.0044)	0.0016)	(0.0063)	(0.402)
0.07 mmol Nd^{3+}	5.8371	8.1607	7.5097	329.33
0.01 mmol Nd^{3+}	(0.0133)	(0.0063)	(0.0139)	(1.063)
0.03 mmol Nd^{3+}	5.8347	8.1571	7.4941	328.16
0.05 mmol Nd^{3+}	(0.0051)	(0.0031)	(0.0055)	(0.404)
0.07 mmol Nd^{3+}	5.8405	8.1666	7.4987	329.39
0.01 mmol Nd^{3+}	(0.0064)	(0.0022)	(0.0066)	(0.503)

Interplanar spacing (d) data for pure and Eu^{3+} and Nd^{3+} doped Bi_2O_3 calculated from Bragg's equation ($n\lambda=2d_{hkl}\sin\theta$) and results summarized in tables 2 and 3. It is clear that the d values were nearly constant with doping Eu^{3+} and Nd^{3+} into Bi_2O_3 .

Table 2. Interplanar spacing (d) data for the Eu^{3+} doped Bi_2O_3 samples.

	Pure Bi_2O_3	1 mmol	3 mmol	5 mmol	7 mmol
d (\AA)	3.25	3.25	3.26	3.26	3.25
2θ ($^\circ$)	27.42	27.42	27.36	27.36	27.42

Table 3. Interplanar spacing (d) data for the Nd^{3+} doped Bi_2O_3 samples.

	Pure Bi_2O_3	1 mmol	3 mmol	5 mmol	7 mmol
d (\AA)	3.25	3.248	3.248	3.248	3.248
2θ ($^\circ$)	27.42	27.42	27.42	27.42	27.42

3.2. Morphology analysis

Morphologies of as-prepared nanomaterials were characterized by FESEM. FESEM images of the synthesized Eu^{3+} and Nd^{3+} doped bismuth oxides are given in figures 3-6 and 7-10, respectively. It can be

observed that these materials have rod like and particle structures. Figures 3-6 show that with changing the dopant amount, the morphology of the obtained materials are still in rod structure, however, there is another morphology that is nanoparticle.

Figure 3 shows that the size of particles is about 50 – 70 nm (figure 3a). It is found that the width of the rod structures is about 1.5 μm (figure 3c). Figure 4 shows that with increasing the dopant amount, the morphology is nearly unchanged. However, the size of particles is decreased to 30 – 50 nm (figure 4c) and the width of the rods is decreased to about 1 μm (figure 4b).

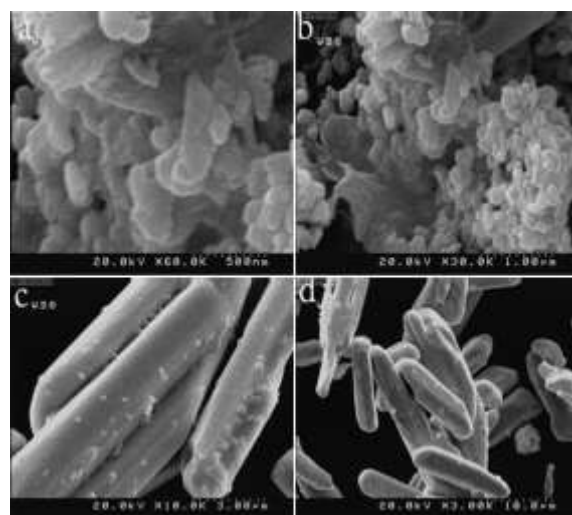
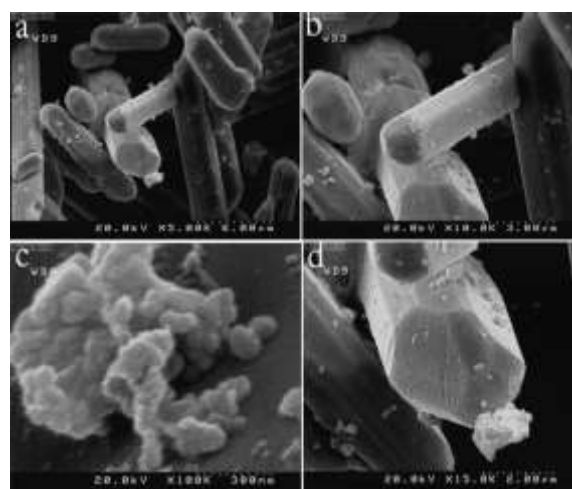
**Fig. 3.** FESEM images of $\text{Bi}_{1.99}\text{Eu}_{0.01}\text{O}_3$.**Fig. 4.** FESEM images of $\text{Bi}_{1.97}\text{Eu}_{0.03}\text{O}_3$.

Figure 5 shows that with increasing the dopant amount to 0.05 mmol, there is an apparent change in the

morphology of the obtained materials. The particles are diminished and the sizes of the rods are different. It was found that the width and length of the small rods are about 50 nm and 150 – 200 nm, respectively.

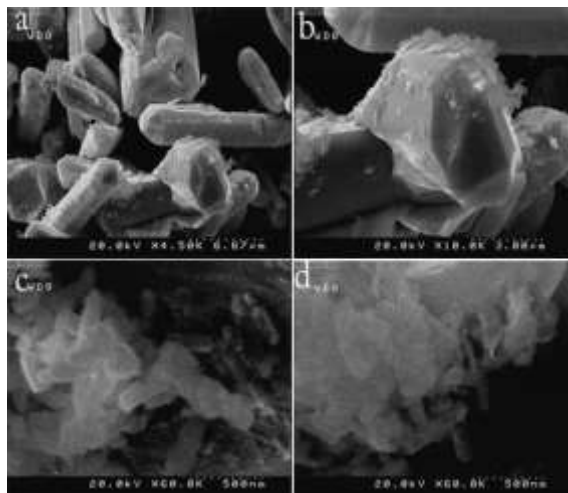


Fig. 5. FESEM images of $\text{Bi}_{1.95}\text{Eu}_{0.05}\text{O}_3$.

Figure 6 shows the FESEM images of the Eu^{3+} - doped Bi_2O_3 nanomaterials. It was found that with increasing the Eu^{3+} amount, the morphology of the obtained materials were homogeneous micro rods. Besides, the particles grown on the surface of the rods were in lower density than that of figure 4. However, the widths of the rods are about 1 μm and the diameter sizes of the particles are about 100 nm.

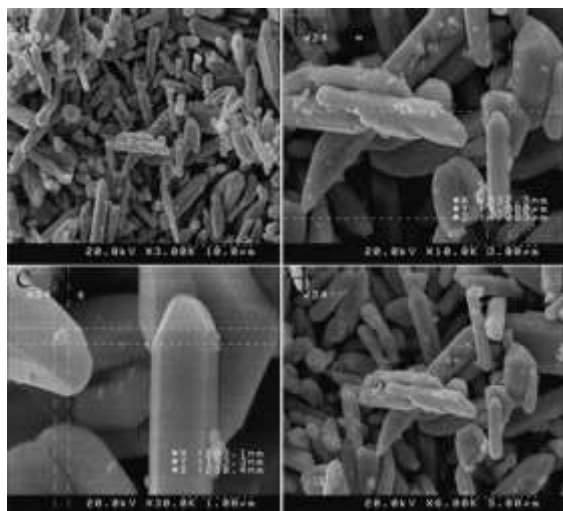


Fig. 6. FESEM images of $\text{Bi}_{1.93}\text{Eu}_{0.07}\text{O}_3$.

Figure 7 shows that with doping Nd^{3+} into Bi_2O_3 , the morphology of the obtained materials were non-

homogeneous micro rods and particles. It is clear from figure 7 a and b that the rods length and thickness sizes are different from each other. However, from figure 7 c and d, it was found that there are some particles with no certain morphology. The particles sizes are found to be about 80 – 100 nm.

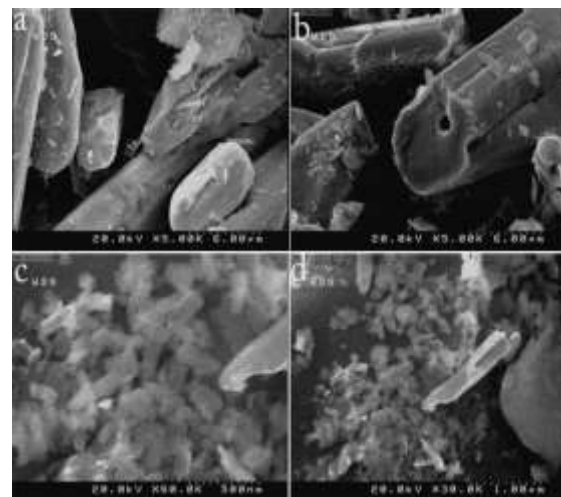


Fig. 7. FESEM images of $\text{Bi}_{1.99}\text{Nd}_{0.01}\text{O}_3$.

Figure 8 shows that with increasing the dopant amount to $x=0.03$ mmol, it was found that the morphologies of the obtained materials are still rod and particle. However, it is obvious that the rods and particles sizes are homogeneous. It was found that the particles sizes are about 50-60 nm.

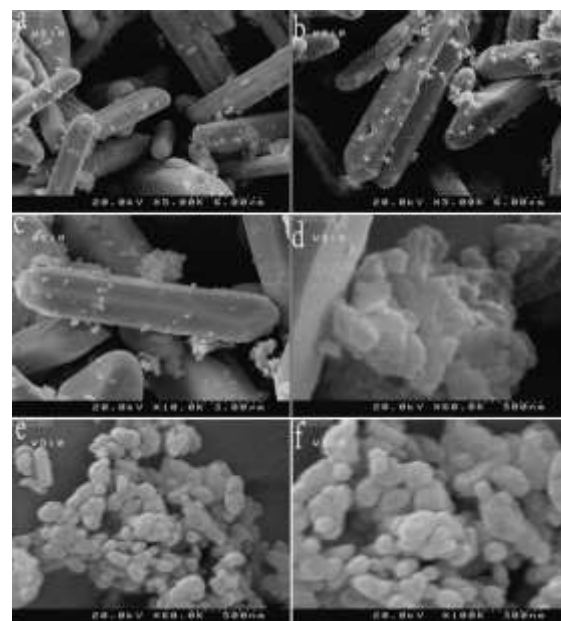


Fig. 8. FESEM images of $\text{Bi}_{1.97}\text{Nd}_{0.03}\text{O}_3$.

Figure 9 shows the FESEM images of the obtained materials when doping $x=0.05$ mmol of Nd^{3+} into Bi_2O_3 . It was found that the morphologies of the materials are rod (figure 9a and b), particle (figure c and d) and flower (figure e) structures. It is clear that the thickness size of the rod structure is about 500 nm, the diameter size of the particles are about 30-50 nm. Besides, the flower size is about 3 μm . It was found that the flower has been formed from the petals cutting each other.

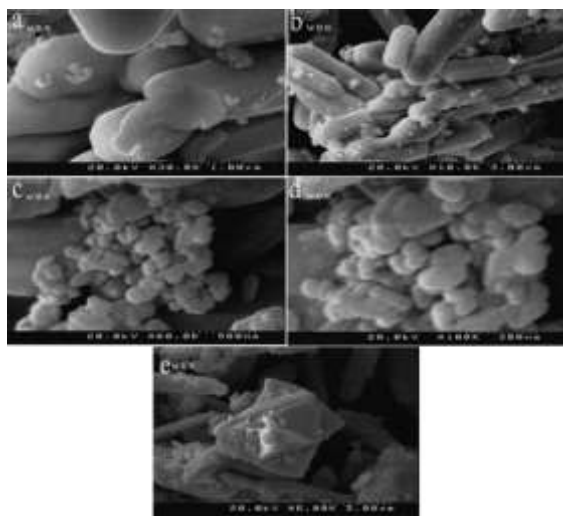


Fig. 9. FESEM images of $\text{Bi}_{1.95}\text{Nd}_{0.05}\text{O}_3$.

Figure 10 shows that with increasing the dopant amount, the morphology of the obtained materials are rod and particles. However, it was found that the particles are in the form of rod and spherical particles (figure 10a and d). It was found that the diameter size of the particles are about 100 – 150 nm and the thickness size of the rods are about 100 nm and length size of them are about 150 nm.

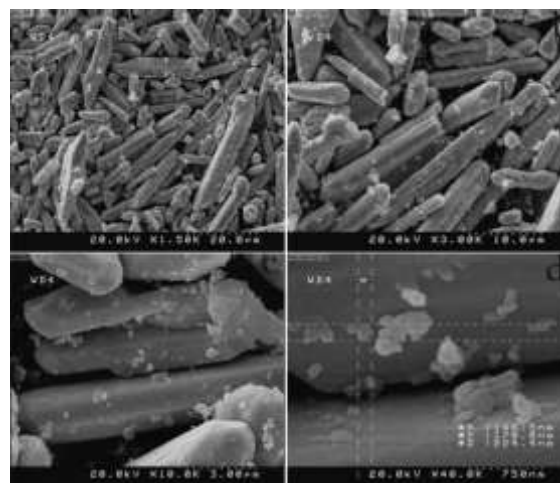


Fig. 10. FESEM images of $\text{Bi}_{1.93}\text{Nd}_{0.07}\text{O}_3$.

3.3. Elemental analysis

The energy dispersive X-ray spectrum (EDS) for the sample doped with 0.07 mmol of Eu_2O_3 and 0.07 mmol of Nd_2O_3 is illustrated in figures 11 and 12 respectively. The respective energy positions and the specific X-ray lines from various elements are also indicated. The EDS spectra confirm the presence of oxygen (O), Bismuth (Bi), Europium (Eu) and Neodymium (Nd) elements in $\text{Bi}_{1.93}\text{Eu}_{0.07}\text{O}_3$ and $\text{Bi}_{1.93}\text{Nd}_{0.07}\text{O}_3$ nanomaterial respectively. Furthermore these analyses verify the doping of Eu^{3+} and Nd^{3+} in Bi_2O_3 nanomaterial. The Normalized elemental analyses of the doped nanomaterials are summarized in table 4.

Table 4. Elemental analyses data of the Eu^{3+} , Nd^{3+} doped Bi_2O_3 .

dopant	Normalized element analysis (wt%)
Eu^{3+}	1.24
Nd^{3+}	1.39

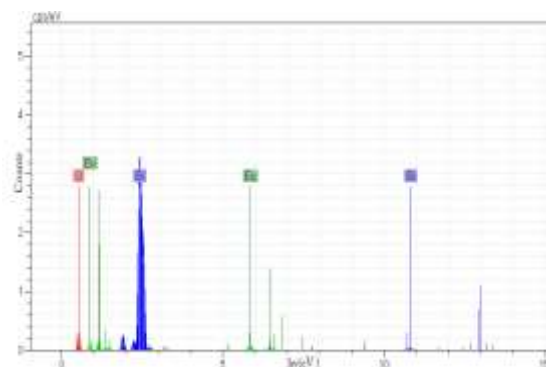


Fig. 11. EDS spectrum of the hydrothermally synthesized $\text{Bi}_{2-x}\text{Eu}_x\text{O}_3$ nanomaterial, where $x = 0.07$ mmol.

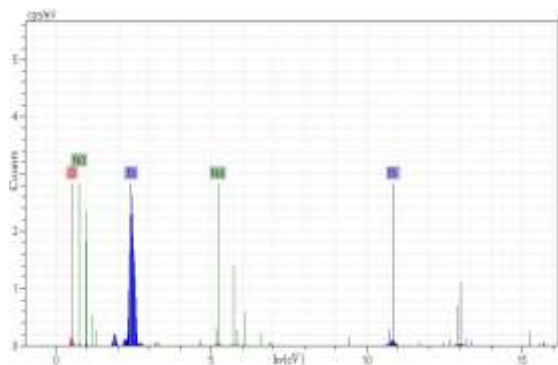


Fig. 12. EDS spectrum of the hydrothermally synthesized $\text{Bi}_{2-x}\text{Nd}_x\text{O}_3$ nanomaterial, where $x = 0.07$ mmol.

4. Conclusion

In this work, the Eu^{3+} and Nd^{3+} - doped Bi_2O_3 nanomaterials were synthesized successfully via mild hydrothermal method. PXRD patterns showed that the synthesis was done successfully. FESEM images showed the rod, particle and flower type structures in the as-synthesized materials. Elemental analysis showed that the doping limitation for Eu^{3+} doped Bi_2O_3 was 1.24 wt% and for Nd^{3+} - doped Bi_2O_3 was 1.39 wt%. Also, cell parameter refinements and interplanar spacing of the doped nanomaterials were calculated by Bragg's equation and celref software.

References

[1] K. Brezesinski, R. Ostermann, P. Hartmann, J. Perlich and T. Brezesinski, *Chem Mater*, **22** (2010) 3079.
 [2] J.-y. Xia, M.-t. Tang, C. Cui, S.-m. Jin and Y.-m. Chen, *T. Nonferr. Metal. Soc.*, **22** (2012) 2289.
 [3] A. Feldman, W.S. Brower Jr and D. Horowitz, *Appl. Phys. Lett.*, **16** (1970) 201.
 [4] A. Pan and A. Ghosh, *J. Non Cryst. Solids*, **271** (2000) 157.
 [5] E.Y. Wang and K.A. Pandelišev, *J. Appl. Phys.*, **52** (1981) 4818.
 [6] M. Schuisky and A. Hårsta: *Chem. Vap. Deposition*, **2** (1996) 235.

[7] M. Yashima and D. Ishimura, *Chem. Phys. Lett.*, **378** (2003) 395.
 [8] F. Qin, H. Zhao, G. Li, H. Yang, J. Li, R. Wang, Y. Liu, J. Hu, H. Sun and R. Chen, *Nanoscale*, **6** (2014) 5402.
 [9] A. Cabot, A. Marsal, J. Arbiol and J. Morante, *Sens Actuators B chem.*, **99** (2004) 74.
 [10] X. Gou, R. Li, G. Wang, Z. Chen and D. Wexler, *Nanotech.*, **20** (2009) 495501.
 [11] K.T. Lee, A.A. Lidie, S.Y. Jeon, G.T. Hitz, S.J. Song and E.D. Wachsman, *J. Mater. Chem. A*, **1** (2013) 6199.
 [12] M. Schlesinger, S. Schulze, M. Hietschold and M. Mehring, *Dalton Trans.*, **42** (2013) 1047.
 [13] S. Wu, J. Fang, X. Xu, Z. Liu, X. Zhu and W. Xu, *Photochem. Photobio.*, **88** (2012) 1205.
 [14] S. Wu, J. Fang, W. Xu and C. Cen, *J. Chem. Tech. Biotech.*, **88** (2013) 1828.
 [15] J. Krishna Reddy, B. Srinivas, V. Durga Kumari and M. Subrahmanyam, *Chem. Cat. Chem.*, **1** (2009) 492.
 [16] J. Zhang Li, J. Bo Zhong, J. Zeng, F. Mei Feng and J. Jin He, *Mater. Sci. Sem. Proc.*, **16** (2013) 379.
 [17] N.O. Kalaycioglu and E. Çırçır, *Metal-Org. Nano-Metal Chem.*, **42** (2012) 398.
 [18] A. Aytimur, İ. Taşçıoğlu, M. Arı, İ. Uslu, Y. Dağdemir, S. Durmuş and Ş. Altındal, *J. sol-gel sci. tech.*, **66** (2013) 317.
 [19] H. Liu, M. Luo, J. Hu, T. Zhou, R. Chen and J. Li, *Appl. Catal. B: Env.*, **140** (2013) 141.
 [20] S. Ohara and Y. Kuroiwa, *Opt. Express*, **17** (2009) 14104.
 [21] P. Šulcová and E. Proklešková: *J. Min. Met, Section B: Metallurgy*, **44** (2008) 27.

- [22] P. Šulcová, E. Proklešková, P. Bystrzycki and M. Trojan, *J. Ther. Anal. Cal*, **100** (2010) 65.
- [23] İ. Taşçıoğlu, M. Arı, I. Uslu, S. Koçyiğit, Y. Dağdemir, V. Corumlu and Ş. Altındal, *Ceram. Int*, **38** (2012) 6455.
- [24] J. Xie, X. Lü, M. Chen, G. Zhao, Y. Song and S. Lu, *Dyes Pigment*, **77** (2008) 43.
- [25] Y. Dai and L. Yin, *J. Alloy. Compd*, **563** (2013) 80.
- [26] T. Sreethawong, S. Chavadej, S. Ngamsinlapasathian and S. Yoshikawa, *Solid State Sci*, **10** (2008) 20.
- [27] B. Umesh, B. Eraiah, H. Nagabhushana, B. Nagabhushana, G. Nagaraja, C. Shivakumara and R. Chakradhar, *J. Alloy. Compd*, **509** (2011) 1146.
- [28] R. Bazzi, M. Flores-Gonzalez, C. Louis, K. Lebbou, C. Dujardin, A. Brenier, W. Zhang, O. Tillement, E. Bernstein and P. Perriat, *J. Lumin*, **102** (2003) 445.
- [29] C. Soliman, *Neodymium oxide: Nucl Instrum Meth B*, **251** (2006) 441.
- [30] W. Que, C. Kam, Y. Zhou, Y. Lam and Y. Chan, *J. Applied Phys*, **90** (2001) 4865.
- [31] A. Kosola, J. Päiväsaari, M. Putkonen and L. Niinistö, *Thin Solid Films*, **479** (2005) 152.
- [32] M. Zawadzki and L. Kepiński, *J. alloy. Compd*, **380** (2004) 255.
- [33] Z.-L. Wang, G.-R. Li, Y.-N. Ou, Z.-P. Feng, D.-L. Qu and Y.-X. Tong, *J. Phys. Chem. C*, **115** (2010) 351.
- [34] H. Li, Y. Sheng, H. Zhang, J. Xue, K. Zheng, Q. Huo and H. Zou, *Powder Tech*, **212** (2011) 372.
- [35] G. Wang, H. Zou, L. Gong, Z. Shi, X. Xu and Y. Sheng, *Powder Tech*, **258** (2014) 174.
- [36] F. Ren and D. Chen, *Powder Tech*, **194** (2009) 187.
- [37] G. Li, Y. Lai, W. Bao, L. Li, M. Li, S. Gan, T. Long and L. Zou, *Powder Tech*, **214** (2011) 211.
- [38] S. Yilmaz, O. Turkoglu, M. Ari and I. Belenli, *Cerâmica*, **57** (2011) 185.
- [39] A. Kar and A. Patra, *J. Phys. Chem. C*, **113** (2009) 4375.
- [40] D. Ye, D. Li, W. Chen, Y. Shao, G. Xiao, M. Sun and X. Fu, *Res. Chem. Int*, **35** (2009) 675.
- [41] T. Dong, Z. Li, Z. Ding, L. Wu, X. Wang and X. Fu, *Mater. Res. Bul*, **43** (2008) 1694.
- [42] M. Behzad, M. sabaghian, S. M. Sajjadi, *J. advan. Mater. Proc*, **3** (2015) 65.
- [43] Y. Li, M. Ge, J. Li, J. Wang and H. Zhang, *Cryst. Eng. Comm*, **13** (2011) 637.
- [44] B. Zhaorigetu, G. Ridi and L. Min, *J. alloy. Compd*, **427** (2007) 235.